Original Article

Test-retest precision of brain metabolites in healthy participants using ^{31}P-MRS and ^{1}H MEGA-PRESS on a 3T multi-nuclear MRI system

Shuang Hu[1], Su Yan[1], Yan Xie[1], Hongquan Zhu[1], Yujie Ding[1], Yuanhao Li[1], Xiaoxiao Zhang[2], Wenzhen Zhu[1]

[1]Department of Radiology, Tongji Hospital, Tongji Medical College, Huazhong University of Science and Technology, Wuhan, China; [2]Clinical Technical Solutions, Philips Healthcare, Beijing, China

Contributions: (I) Conception and design: S Hu, S Yan, H Zhu, W Zhu; (II) Administrative support: X Zhang, W Zhu; (III) Provision of study materials or patients: S Hu, Y Xie; (IV) Collection and assembly of data: Y Ding; (V) Data analysis and interpretation: S Hu, S Yan, Y Li; (VI) Manuscript writing: All authors; (VII) Final approval of manuscript: All authors.

Correspondence to: Wenzhen Zhu, PhD. Department of Radiology, Tongji Hospital, Tongji Medical College, Huazhong University of Science and Technology, No. 1095, Jiefang Road, Wuhan 430030, China. Email: zhuwenzhen8612@163.com.

Background: Magnetic resonance spectroscopy (MRS) enables the non-invasive quantification of brain metabolites, and its reliability is crucial for accurate interpretation of disease state. This study assessed the test-retest precision of phosphorus-31 (^{31}P)-MRS and hydrogen (^{1}H)-MEscher-GArwood Point RESolved Spectroscopy (MEGA-PRESS) in measuring ^{31}P metabolites, γ-aminobutyric acid (GABA), and glutathione (GSH) using a 3T multi-nucleus magnetic resonance imaging (MRI) system.

Methods: In total, 32 participants, who underwent two scanning sessions within three days, using two dimensional (2D)-chemical shift imaging (CSI)-^{31}P-MRS and ^{1}H-MEGA-PRESS sequences, were enrolled in the study. γ-aminobutyric acid and macromolecules (GABA+), glutamate and glutamine (Glx), GSH, and 12 ^{31}P metabolites were analyzed using the MATLAB-based tool Gannet and jMRUI software. Precision was assessed based on the coefficients of variation (CVs) and Bland-Altman plots.

Results: The results revealed that potential of hydrogen (pH) and phosphocreatine (PCr) showed the greatest stability as evidenced by low CVs, suggesting reliable measurements across sessions. The adenosine triphosphates (ATPs) showed considerable stability. Conversely, metabolites, such as phosphomonoesters (PMEs) and phosphodiesters (PDEs), located to the left of PCr, showed reduced stability, while glycerophosphatidylcholine (GPTC) had the highest CV, indicating significant variability in clinical practice. Among the various brain regions, intermediate areas such as the temporal lobe and thalamus exhibited greater stability than peripheral regions such as the frontal and occipital lobes. Single-voxel MEGA-PRESS measurements showed that Glx and GABA+ had higher precision than GSH.

Conclusions: Both the ^{31}P-MRS and ^{1}H-MEGA-PRESS sequences showed high precision in measuring brain metabolites, but some metabolites showed higher stability than others. These results are crucial for exploring the clinical and research applications of these methods, and provide a solid foundation for subsequent investigations.

Keywords: Phosphorus-31 magnetic resonance spectroscopy (^{31}P-MRS); MEscher-GArwood Point RESolved Spectroscopy (MEGA-PRESS); γ-aminobutyric acid (GABA); glutathione (GSH); test-retest

Submitted Sep 02, 2024. Accepted for publication Mar 03, 2025. Published online Mar 28, 2025.
doi: 10.21037/qims-24-1853
View this article at: https://dx.doi.org/10.21037/qims-24-1853

Introduction

Magnetic resonance spectroscopy (MRS) has been established as a clinical research tool for brain disorders (1). The vast majority of MRS applications performed today are based on exciting magnetic moment of hydrogen (^{1}H) nuclei to detect low-concentration metabolite signals; for example, γ-aminobutyric acid (GABA) and glutathione (GSH) (2). Beyond ^{1}H, multi-nuclear magnetic resonance imaging (MRI) systems frequently employ phosphorus 31 (^{31}P) as a key nucleus for spectroscopic analysis. ^{31}P-MRS has been employed as a tool to investigate intracellular pH and metabolism *in vivo*, providing complementary information not available from ^{1}H-MRS (3-5).

The MEscher-GArwood Point RESolved Spectroscopy (MEGA-PRESS) sequence uses J-editing pulses, specifically designed for the accurate detection of low-concentration J-coupled metabolites. It is particularly widely used for the quantification of GABA and GSH in 3T MRI systems (6). J-editing entails subtracting two spectra and applying a frequency-selective inversion to a target resonance. However, this approach is susceptible to artifacts caused by subject movement or scanner instability (7).

Previous research has shown the strong test-retest reliability of GABA and GSH MRS in the posterior cingulate cortex (6), occipital cortex (8), and primary motor cortex (9), with coefficients of variation (CVs) ranging from 3% to 5%. Several other studies have examined other areas, including the thalamus (10) and the dorsolateral prefrontal cortex (11), reporting CVs below 10%. Two reliability studies investigated the dorsal anterior cingulate cortex (dACC), and reported CVs ranging from 7.3% to 25.4% (12,13). The dACC is an important hub region involved in prospection, threat coping, and emotional regulation (14). Its function is implicated in various disease processes, including neurodegeneration (15) and pain (16), and it is a highly relevant target for detailed metabolic examination (17). Given the notable variability in test-retest findings, this study sought to ascertain the true reliability of GABA and GSH quantification using MEGA-PRESS.

^{31}P-MRS provides insights into the cellular environment, such as the cell membrane structure, bioenergetic processes, oxidative phosphorylation, and intracellular pH and magnesium levels. It enables the detection of various metabolites such as phosphomonoesters (PMEs), which consist of phosphoethanolamine (PE) and phosphocholine (PC), and phosphodiesters (PDEs) including glycerophosphoethanolamine (GPE) and glycerophosphocholine (GPC). Additionally, it can measure inorganic phosphate (Pi), glycerophosphatidylcholine (GPTC), phosphocreatine (PCr), and adenosine triphosphate (ATP) (18). Changes in metabolic ratios, including Pi/ATP and PCr/ATP, have been linked to conditions such as Parkinson's disease, brain tumors, multiple sclerosis, and psychiatric disorders (19-22).

^{31}P-MRS has not yet gained clinical acceptance due to unresolved technical issues. The lower gyromagnetic ratio of ^{31}P nuclei compared to ^{1}H nuclei causes lower signal intensity, and the nuclear sensitivity and concentration of ^{31}P metabolites are also significantly lower than those for ^{1}H metabolites, resulting in a weaker signal (23). Additionally, scalar (J)-coupling interactions between nearby ^{31}P and ^{1}H nuclei split the spectral lines of phosphorus metabolites and reduce their intensities (24). The reproducibility of experiments has also attracted increasing concern. As summarized in *Table 1*, a 7T ^{31}P-MRS investigation reported CVs ranging from 8.1% to 28.4% across various brain regions (25). Conversely, another study conducted with 10 volunteers using a 3T MRI system reported CVs for various brain regions that were consistently below 10% (26). Studies with small sample sizes may result in inaccurate conclusions and findings. Thus, it is crucial to conduct more extensive studies with larger cohorts to ensure ^{31}P-MRS reliability.

In this study, using a 3T multi-nuclear MRI system, we assessed the test-retest precision of ^{31}P-MRS and ^{1}H-MEGA-PRESS sequences. Since the edited GABA and macromolecule (MM) signals at ~3 ppm overlap completely and are indistinguishable, we labeled the total GABA and MM signals as GABA+ (7). Glx refers to the sum of glutamate and glutamine concentration. The frontal, temporal, thalamus and occipital lobes were chosen as the volumes of interest (VOIs) for ^{31}P-MRS to facilitate a comprehensive examination of metabolic profiles across these critical brain regions. We present this article in accordance with the STARD reporting checklist (available at https://qims.amegroups.com/article/view/10.21037/qims-24-1853/rc).

Methods

Participants

The study was conducted in accordance with the Declaration of Helsinki (as revised in 2013) and approved by the Institutional Review Board of Tongji Hospital

Table 1 Previous GABA/GSH MEGA-PRESS and ^{31}P MRS repeatability and reliability studies

Reference	Field strength	Nuclear	Brain region	N	Metabolite ratio	CV values
Baeshen *et al.* [2020] (6)	3T	^{1}H	PCC	18	GABA; Glx	GABA: CV =8.8%; Glx: CV =5.1%
Anton *et al.* [2022] (8)	3T	^{1}H	PMC; OCC	10	GSH	Intraday CV =3.3% in PMC and 2.4% in OCC; CVs at 1 month apart: 4.6% in PMC; 7.8% in OCC
Greenhouse *et al.* [2016] (9)	3T	^{1}H	OCC; PMC	28	GABA+	PMC: CV =3.9%; OCC: CV =5.3%
Ma *et al.* [2020] (10)	3T	^{1}H	Thalamus	14	GABA+/tCr; Glx/tCr	CV =6.3%; CV =2.35%
Duda *et al.* [2021] (11)	3T	^{1}H	rACC; DLPFC	21	GABA+/tCr; GABA+/water	GABA+/tCr: 4.6% for dlPFC; 8.0% for rACC; GABA+/water: 4.0% for dlPFC; 7.5% for rACC
Hupfeld *et al.* [2023] (12)	3T	^{1}H	dACC	20	GABA+	CV =25.4%
Song *et al.* [2022] (13)	3T	^{1}H	dACC	12	GSH	CV =7.3%
Lagemaat *et al.* [2016] (25)	7T	^{31}P	Multi-regions	7	PE/PC; Pi/PCr; GPE/GPC; PE/PCr; PCr/γATP; NAD/αATP	8.1%< CV <28.4%
Parasoglou *et al.* [2022] (26)	3T	^{31}P	Multi-regions	10	PCr/ATP; Pi/ATP; PME/PDE; pH	CV <10%

CV, coefficient of variation; dlPFC, dorsolateral prefrontal cortex; GPE, glycerophosphoethanolamine; GPC, glycerophosphocholine; GABA+, γ-aminobutyric acid + macromolecules; Glx, glutamate + glutamine; GSH, glutathione; NAD, nicotinamide adenine dinucleotide; PMC, primary motor cortex; OCC, occipital cortex; PE, phosphoethanolamine; PCC, posterior cingulate cortex; PC, phosphocholine; Pi, inorganic phosphate; PCr, phosphocreatine; γ-, α-, β-ATP, α-, β-, γ-adenosine triphosphate; PME, phosphomonoester; PDE, phosphodiester; tCr, total creatine; rACC, rostral anterior cingulate cortex.

of Tongji Medical College of Huazhong University of Science and Technology (No. TJ-IRB20231102), and all participants provided written informed consent before the commencement of this study. From November 2023 to February 2024, 32 healthy participants (26.84±5.46 years, 12 men) visited the laboratory on two occasions in 3 days (from 1 to 3 days). To minimize potential circadian rhythm effects, all testing sessions were scheduled at the same time of day for every participant (27). Attempts were made to avoid scheduling the female subjects during their menstrual cycles. Additionally, the participants were instructed to refrain from strenuous exercise, and abstain from consuming caffeine or alcohol for 24 hours before the test (8).

MRS acquisition

The data were acquired on a 3.0-Tesla magnetic resonance scanner (Philips Elition X, Best, The Netherlands) with a 32-channel head coil and a dual-tuned (^{1}H/^{31}P) head coil (Rapid Biomed, Germany). The scanning protocol included a three-dimensional T1-weighted structural image [T_1 turbo field echo sequence, repetition time/echo time (TR/TE): 6.6/3.0 ms, voxel size: 1×1×1 mm^3, and acquisition time: 3 min 20 seconds] was employed to position the voxel within the dACC and to quantify the gray matter (GM), white matter (WM), and cerebrospinal fluid (CSF) compositions within the voxel for each participant. To ensure consistent voxel placement, anatomical landmarks served as the reference points; the voxel was aligned parallel to the superior anterior border of the genu of the corpus callosum, with its anterior edge terminating at the anterior margin of the corpus callosum. Additionally, in both the coronal and axial planes, the voxel was parallel to the sagittal suture of the brain (*Figure 1*). The ^{1}H-MRS data were acquired using GABA-edited and GSH-edited MEGA-PRESS sequences.

The MEGA-PRESS editing strategies referenced experts' consensus recommendations as described by Choi

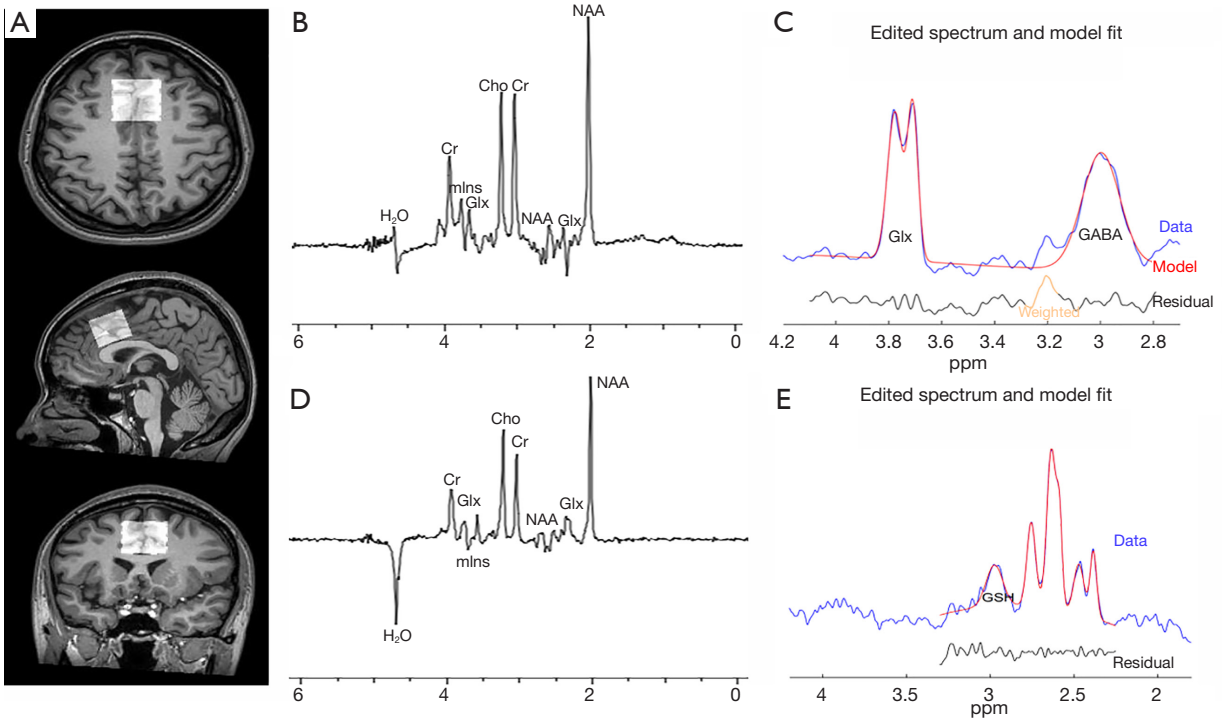

Figure 1 The representative spectrum and voxel location. (A) Illustration of the MEGA-PRESS MRS voxel position. The MRS voxel was placed in the anterior cingulate cortex region. (B) GABA-nonedited PRESS raw data. (C) GABA-edited spectrum and model fit. (D) GSH-non-edited PRESS raw data. (E) GSH-edited spectrum and model fit. Cho, choline; Cr, creatine; Glx, glutamate + glutamine; mIns: myo-inositol; GABA, γ-aminobutyric acid; GSH, glutathione; MEGA-PRESS, MEscher-GArwood Point RESolved Spectroscopy; MRS, Magnetic resonance spectroscopy; NAA, n-acetyl-aspartate.

et al. (7), and are reported as per the minimum reporting standards for *in vivo* MRS (28). Details of the MEGA-PRESS parameters are provided in Table S1. The GABA+, Glx, and GSH concentrations were quantified using both total creatine (Cr) and the relaxation correction water as the internal reference signal. Each MEGA-PRESS scan required a total acquisition time of 8 min 48 seconds, which included 8 min 32 seconds for water-suppressed spectra and an additional 16 seconds for water non-suppressed spectra.

Following ^{1}H-MRS acquisition, we switched to the ^{1}H/^{31}P birdcage coil and repositioned the participant for the ^{31}P-MRS sequence. Another 3D T1-weighted structural image (TR/TE: 4.3/1.97 ms, voxel size: 2×2.15×2 mm^3, and acquisition time: 3 min 39 seconds) was acquired for the placement of the two-dimensional (2D) chemical shift imaging (CSI) ^{31}P-MRS voxels. 2D CSI ^{31}P-MRS used vendor pre-set adiabatic pulses, and the acquisition parameters were as follows: TR/TE: 3,500/0.22 ms, number of signal averages: 6, sampling points: 2,048, spectral bandwidth: 3,000 Hz, flip angle: 360°, slice thickness: 20 mm, field of view: 240×240 mm^2, acquired voxel sizes: 40×40×20 mm^3 and, following k-space filtering and zero filling using a reconstruction matrix of 16×16, reconstructed voxel size: 15×15×20 mm^3. The spectral signal-to-noise ratio (SNR) and line shapes were enhanced through the application of an automated first-order pencil beam shim, combined with WALTZ-4 broadband heteronuclear decoupling and the nuclear Overhauser effect. The total acquisition time was 9 min 24 seconds for ^{31}P-MRS. The thalamus was aligned at the isocenter of the CSI grid, which was positioned mid-sagittal along the x-axis. The grid was then tilted to align parallelly with the anterior commissure-posterior commissure line in the sagittal (yz) plane, with its lower edge adjusted to intersect the inferior colliculus (*Figure 2*).

In the initial scan session, a screen capture of the voxel placement (in three orthogonal planes) was recorded. During the subsequent session, this image served as a reference guide to visually reposition the voxel in a nearly identical location for the follow-up scan. All the scan tasks

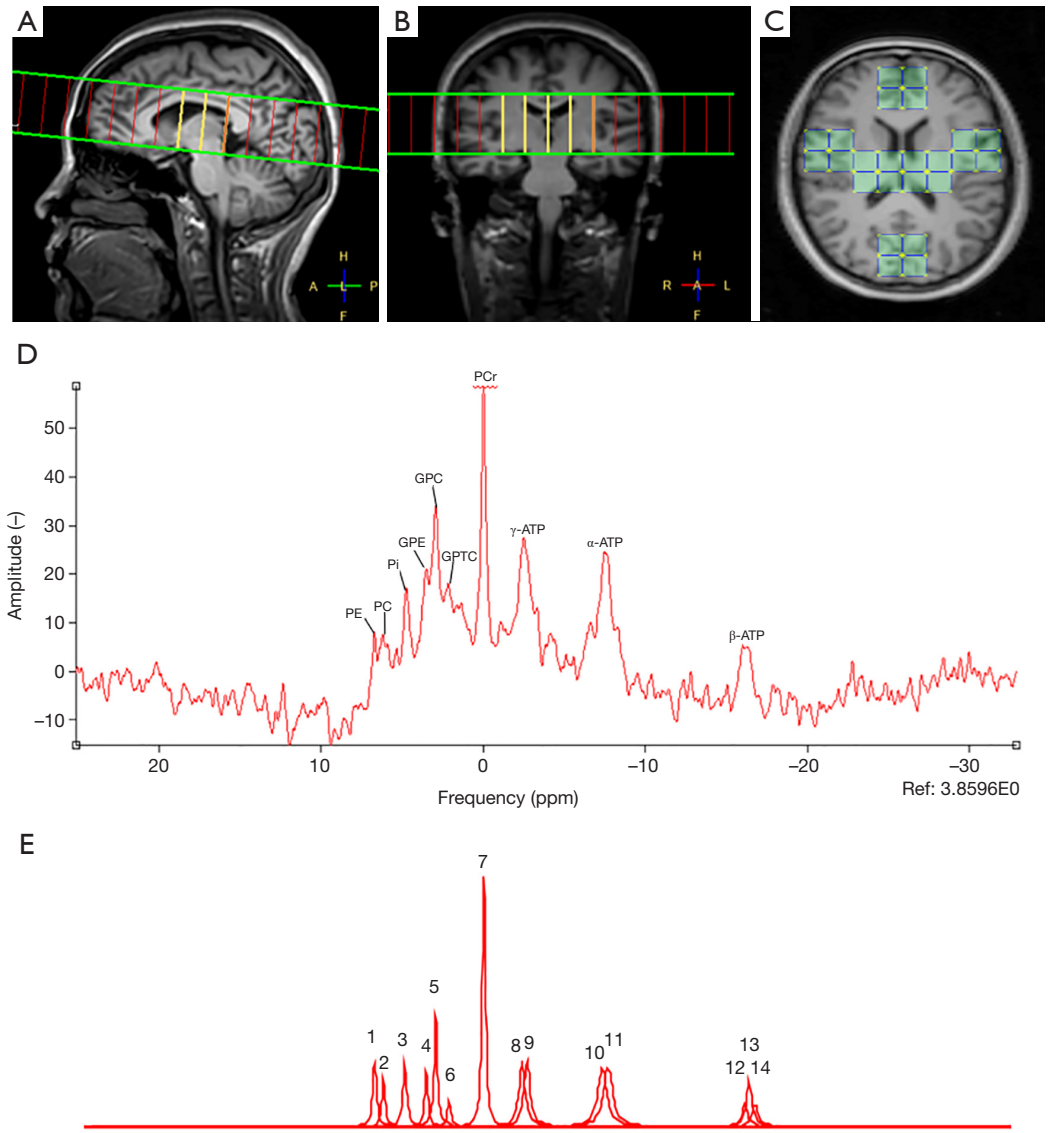

Figure 2 Anatomical localization of the spectroscopic grid and example of fit of a brain spectrum acquired from the bilateral temporal lobe of a healthy volunteer. Sagittal (A), coronal (B), and axial (C) images illustrate the positioning of the spectroscopic grid. An example of a brain spectrum (D) acquired from averaged voxel (highlighted in C); resolved peaks are (from left to right): PE, PC, Pi, GPE, GPC, GPTC, PCr, and the γ α, β phosphates of ATP. (E) Spectral fitting; individual resonances are depicted (1 = PE; 2 = PC; 3 = Pi; 4 = GPE; 5 = GPC; 6= GPTC; 7 = PCr; 8, 9 = γ-ATP; 10, 11 = α-ATP; 12, 13, 14 = β-ATP). GPE, glycerophosphoethanolamine; GPC, glycerophosphocholine; GPTC, glycerophosphatidylcholine; Mg^{2+}, magnesium ion; PE, phosphoethanolamine; PC, phosphocholine; Pi, inorganic phosphate; PCr, phosphocreatine; γ-, α-, β-ATP, α-, β-, γ-adenosine triphosphate.

were carried out by the same neuroradiologist (S.H., with seven years of experience).

Spectroscopic data processing

The MEGA-PRESS data were analyzed using the MATLAB-based Gannet toolbox (version 3.1) (29). Gannet includes multiple modules, with GannetLoad performing zero filling, applying a 3-Hz exponential line broadening, and implementing robust frequency-and-phase correction for individual averages through the spectral registration algorithm (30). To address subtraction artifacts in most

datasets, the "RobustSpecReg" spectral alignment method was used in conjunction with spectral registration to reduce fit error (31). The aligned transients were then averaged to yield the edit-ON and edit-OFF spectra, which were subsequently subtracted to create the GABA/GSH-edited MEGA-PRESS difference spectrum. The SpecReg algorithm was used to align the GABA spectra, and the Cr peak was used as a reference to align the GSH spectra. The GannetFit module was employed for spectral fitting, using a 3-Gaussian model to analyze GABA+ and Glx signal within the 2.79 to 4.1 ppm range. Additionally, a 6-Gaussian model was applied to process GSH spectra between 2.25 and 3.5 ppm, with one Gaussian specifically dedicated to fitting the GSH signal. The creatine peak was fitted in the "OFF" spectrum, while the water signal from the unsuppressed data was modeled using Lorentzian peaks. Additionally, the GannetCoRegister and GannetSegment modules used SPM12 (32) to calculate the volume fractions of GM, WM, and CSF within the tissue. The GannetQuantify module was subsequently executed to derive the metabolite concentrations in institutional units, with adjustments made to account for tissue water content and relaxation effects. GABA+, Glx, and GSH concentrations were reported relative to total Cr and the relaxation correction water. The spectral quality was assessed visually to identify artifacts or inadequate water suppression. Scans with a fit error [calculated as the standard deviation (SD) of the fit residual divided by the model amplitude] exceeding 15%, a threshold commonly recommended in GABA spectroscopy literature, were excluded from further analysis (29,33). Two GABA-edited spectral data and four GSH-edited spectral data were excluded.

The ^{31}P-MRS data were analyzed in the time domain using jMRUI software (version 7.0.3) (34,35). Signal fitting was conducted using the Advanced Method for Accurate, Robust and Efficient Spectral Fitting (AMARES) algorithm to quantify the relative area under each peak. For each participant, voxels from the frontal, temporal, thalamus and pareto-occipital lobe regions were selected as VOIs for further analysis. The manual preprocessing steps included zero- and first-order phasing to achieve purely absorptive line shapes, along with apodization using a 5-Hz filter. The chemical shift of all spectra was calibrated to PCr at 0 parts per million (ppm). A total of 14 resonances were fitted using Lorentzian line shapes. Specifically, γ-ATP and α-ATP were modeled as doublet peaks with amplitudes and line-widths maintained at a 1:1 ratio to each other, while β-ATP was fitted as triplet peaks with amplitude ratios of 0.5:1.0:0.5 and line-width ratios of 1:1:1. Consistent with previous studies, the coupling constants for ATP multiplets were fixed at 18 Hz, and soft constraints were applied to limit ATP line-widths within the range of 5–35 Hz (19,20) (*Figure 2*). Free estimated on line-widths were applied to PCr; the line-widths of PC, GPE, and GPTC were consistent with PCr. While soft constraints on line-widths were applied to PE, Pi (5.0–15.0 Hz) (36). All signal amplitudes were scaled relative to the total phosphorus signal before conducting the statistical analyses. The fit quality was visually evaluated in every instance to eliminate spurious signals, following established consensus guidelines (37). The pH and magnesium ion (Mg^{2+}) concentrations were calculated from the Pi, β-ATP, and PCr frequency, using the inbuilt formulas in the jMRUI software.

Statistical analysis

The precision of GABA+, Glx, GSH, and 12 ^{31}P metabolites were assessed using CVs. This metric was derived by dividing the SD by the mean of the repeated measurements, and is presented as a percentage (8). The Wilcoxon signed-rank test was used to evaluate the GM, WM, and CSF proportions for the MEGA-PRESS voxels between the repeated scans. Bland-Altman plots were generated to assess the consistency between repeated measurements, with the mean of corresponding repeated values plotted on the x-axis and the percentage difference between the repeats displayed on the y-axis.

Results

The Wilcoxon signed-rank test revealed no significant differences in the percentages of GM, WM, and CSF components for both measurements in the MEGA-PRESS sequences (P=0.322, 0.418, and 0.512 for GM, WM, and CSF, respectively). The SNR for MEGA-PRESS was calculated by GABA+, Glx, GSH signal magnitude/noise SD. The mean SNR of GABA+ was 18.856, that of Glx was 24.910, and that of GSH was 8.688. Meanwhile, the SNR of ^{31}P-MRS was calculated by the PCr signal magnitude in the frequency domain/noise SD in the frequency domain. The mean SNR of the frontal lobe was 48.742, that of the temporal lobe was 50.014, that of the thalamus region was 95.313, and that of the pareto-occipital lobe was 64.064.

In the case of MEGA-PRESS, the CVs for GABA+/Cr and GABA+/water were 3.263% and 3.449%, respectively; the CVs for Glx/Cr and Glx/water were 2.275% and 3.151%, respectively; and the CVs for GSH/Cr and GSH/water were 11.904% and 16.525%, respectively. *Figure 1* provides an example of the MEGA-PRESS spectrum, which clearly shows the GABA+ signal, Glx signal, and GSH signal centered at 3.0, 3.8 and 2.95 ppm, respectively. Bland-Altman plots representing the agreement between scans performed on GABA+, Glx, and GSH are shown in *Figure 3*.

In relation to the ^{31}P-MRS spectra, 10 ^{31}P metabolites were fitted using the AMARES algorithm, and the amplitudes were normalized to the total phosphorus signal. PE had a moderate CV across the brain regions, with values ranging from 13.2% in the thalamus to 18.9% in the occipital lobe. PC had moderate to high CVs in the brain regions, with the frontal lobe at 26.3%, the occipital lobe at 24.4%, the temporal lobe at 14.1% and the thalamus at 16.6%. Pi had higher CVs in the frontal lobe (25.4%) and occipital lobe (19.1%), and lower CVs in the temporal lobe (11.1%) and thalamus (15.8%). GPE had higher CVs in the frontal lobe (25.2%) and occipital lobe (27.6%), and the lowest CV in the thalamus (11.0%). GPC had the lowest CVs in the temporal lobe (9.0%) and thalamus (8.6%), and the highest CV in the occipital lobe (19.3%). GPTC had moderate to high CVs, with the frontal lobe at 23.5%, the temporal lobe at 22.1%, and the thalamus at 21.7%, and had the highest CV in the occipital lobe (32.6%), suggesting significant variability in its measurements. PCr had the lowest CVs among all metabolites, indicating its best stability measurements. γ-ATP had the lowest CV in the temporal lobe (5.8%) and the highest CV in the occipital lobe (12.9%). α-ATP had low CVs across all regions, and β-ATP had a slightly higher CV in the occipital lobe (18.0%). The CVs relative to the two scan time points of ^{31}P-MRS in different brain areas are shown in *Table 2*.

The pH values had very low CVs across all brain regions, with a maximum of only 0.3%. Mg^{2+} had the highest CV in the occipital lobe (16.1%) and the lowest CV in the temporal lobe (12.7%). A representative example of the ^{31}P-MRS spectra, together with their corresponding residues, is shown in *Figure 2*. Bland-Altman plots representing the agreement between scans for the ^{31}P-MRS metabolites in the thalamus region are shown in *Figure 4*, and Figures S1-S3.

Discussion

This study assessed the test-retest precision of ^{31}P-MRS and ^{1}H MEGA-PRESS using a 3T multi-nuclear MRI system. Among the metabolites measured by both sequences, some exhibited high stability, while others displayed moderate or less stability, which is significant in understanding their potential applications in clinical research and practice.

Precision of ^{31}P-MRS

In the comparative analysis of the ^{31}P-MRS metabolites, pH and PCr exhibited the highest degree of stability. The energy peaks of ATPs showed a considerable level of stability. Conversely, the peaks located to the left of the PCr, including the PMEs and PDEs, displayed relatively lower stability. Among these, GPTC showed the poorest stability. These results showed a significant variance in the precision of ^{31}P-MRS measurements across different metabolites.

The measurement of the pH value by ^{31}P-MRS is based on the chemical shift difference between Pi and PCr. The high stability of pH may be due to the strict regulation of pH in the physiological environment compared to other metabolites, which explains why pH exhibits a high degree of stability. PCr was identified as the most abundant substance among the measured metabolites, and was characterized by the tallest peak in the brain's ^{31}P-MRS spectra. This peak was referenced to a chemical shift of 0 ppm. PCr plays a critical role in the rapid conversion of adenosine diphosphate to ATP, thereby serving as an "ATP replenisher" that maintains high-energy phosphate stores essential for cellular function. In comparison to the ATP signals, β-ATP exhibited poorer stability than α-ATP and γ-ATP. β-ATP displayed a 1:2:1 triplet pattern due to its coupling with both α-ATP and γ-ATP, and may suffer from broader signals that are more prone to magnetic field inhomogeneities and motion artifacts. Among the peaks to the left of PCr, GPTC had the highest CV. GPTC is the product of the complete hydrolysis of the two fatty acyl groups on PC. It is a water-soluble small molecule substance that can cross the blood-brain barrier and is an important biochemical precursor of the neurotransmitter acetylcholine. The relatively low abundance of GPTC may be a contributing factor to its high CV.

Precision of the MEGA-PRESS sequences

In terms of the test-retest of the MEGA-PRESS sequences,

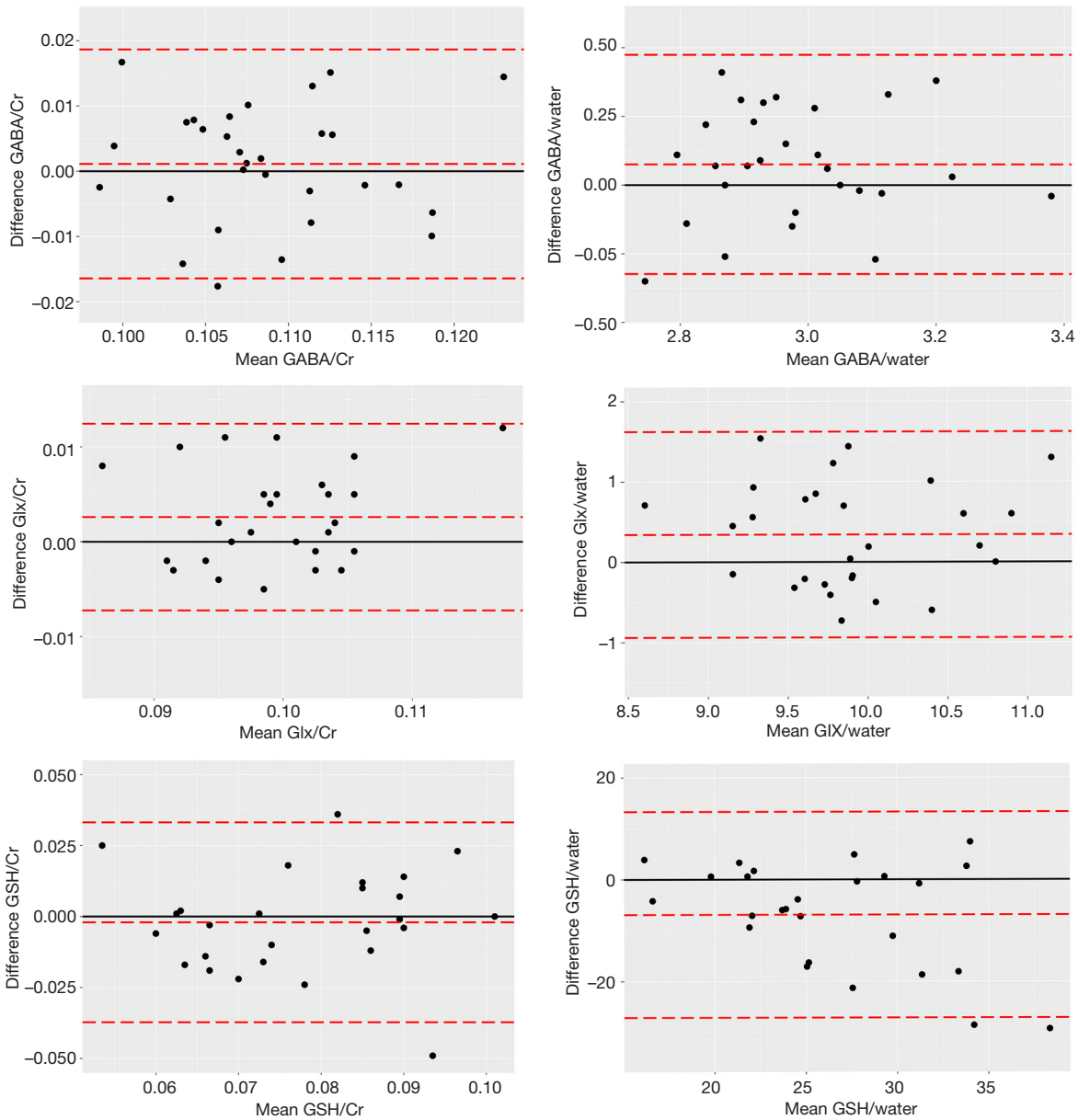

Figure 3 Bland-Altman plots of the two scan time points (1st and 2nd measurements) of MEGA-PRESS. The central red line indicates the mean value of the difference dataset (μ) and the upper and lower red lines are the limits μ+1.96 SD and μ–1.96 SD, respectively. GABA+, Glx, and GSH. GABA, γ-aminobutyric acid; Glx, glutamate + glutamine; GSH, glutathione; MEGA-PRESS, MEscher-GArwood Point RESolved Spectroscopy; SD, standard deviation.

Glx and GABA+ showed better precision than GSH. This was not only reflected by the lower CVs but also by the lower SNR and higher fit error (four samples were excluded). Due to the lower CVs of GSH/Cr, total Cr is recommended as the concentration reference for GSH analysis and quantification. However, as the change of creatine concentration in pathologic conditions is also a concern, it is still recommended that unsuppressed water signals be used as a reference (7). Wijtenburg *et al.* reported same-day measurements of GSH using the MEGA-PRESS sequence, with CVs of 13.5% and 17.1% for GSH/water in the anterior and posterior cingulate regions, respectively (38),

Table 2 The CVs relative to the two scan timepoints (1st and 2nd measurements) of ^{31}P-MRS in different brain areas

Metabolites	Frontal lobe	Temporal lobe	Thalamus	Occipital lobe
PE	13.9	14.4	13.2	18.9
PC	26.3	14.1	16.6	24.4
Pi	25.4	11.1	15.8	19.1
GPE	25.2	13.4	11.0	27.6
GPC	11.6	9.0	8.6	19.3
GPTC	23.5	22.1	21.7	32.6
PCr	4.1	2.9	3.4	7.1
γ-ATP	14.8	5.8	6.0	12.9
α-ATP	7.2	6.5	9.5	8.4
β-ATP	13.1	5.8	11.0	18.0
pH	0.3	0.1	0.2	0.3
Mg^{2+}	14.0	12.7	12.9	16.1

The data were calculated as the ratio between the standard deviation and the mean of repeated measures, and are expressed as a percentage (%). CVs, coefficients of variations; PE, phosphoethanolamine; PC, phosphocholine; Pi, inorganic phosphate; GPE, glycerophosphoethanolamine; GPC, glycerophosphocholine; GPTC, glycerophosphatidylcholine; PCr, phosphocreatine; γ-, α-, β-ATP, α-, β-, γ-adenosine triphosphate; Mg^{2+}, magnesium ion.

which is consistent with our study. However, Anton *et al.* showed the 1-month apart CV for GSH/water was 7.8% in the posterior cingulate region, which is significantly lower than that found in our study. The shorter echo time (120 ms) and more spectral points (2,048 points in free induction decay) may have contributed to the higher SNR (8).

The accuracy of MRS measurements relies on the uniformity of the static magnetic field (B0), radio frequency power calibration, and frequency drift caused by subject movement or system instability (39-41). Due to the long acquisition time, subject motion is a challenge in the adequate spectral and reliable quantification of MRS-derived metabolites. Post-acquisition frequency-and-phase alignment using single-transient spectral data cannot compensate for signal loss resulting from motion or frequency drift during acquisition (7). Even with accurate localization in both scans, the reduction in SNR due to subject movement is inevitable.

The measured repeatability can reliably detect group-wise differences. ^{31}P-MRS has proven useful in monitoring neuronal energy metabolism and metabolic marker changes in disease states (19,42). Schizophrenic patients exhibit changes in PC, PE, and GPC levels compared to healthy controls (21). Parkinson's disease patients show greater variance in the posterior putaminal Pi/ATP ratio compared to controls, and elevated midbrain PCr levels are associated with faster disease progression (19). Alterations in GSH levels have been implicated in neurodegenerative and psychiatric disorders. Patients with mild cognitive impairment and Alzheimer's disease have been shown to have significant GSH depletion and elevated pH levels in the hippocampus (43), while pediatric patients with myelin oligodendrocyte glycoprotein antibody-associated disorders have been shown to have reduced intracellular magnesium and pH associated with ATP line splitting (44).

This study had several limitations. First, the test-retest experiments were limited to healthy participants and did not include disease groups; thus, it is not yet known whether CVs can be used to detect group differences in disease groups. Second, repeatability was only evaluated in the anterior cingulate cortex for MEGA-PRESS. Thus, the generalization of these findings to other brain regions remains uncertain. Third, more ratios of ^{31}P metabolites were not calculated. However, the ratios have been used in many reports to represent energy metabolism. Finally, while the participants were instructed to avoid alcohol and caffeine for 24 hours before each scan, their typical dietary patterns were not documented. Nor was caffeine intake between the two visits monitored.

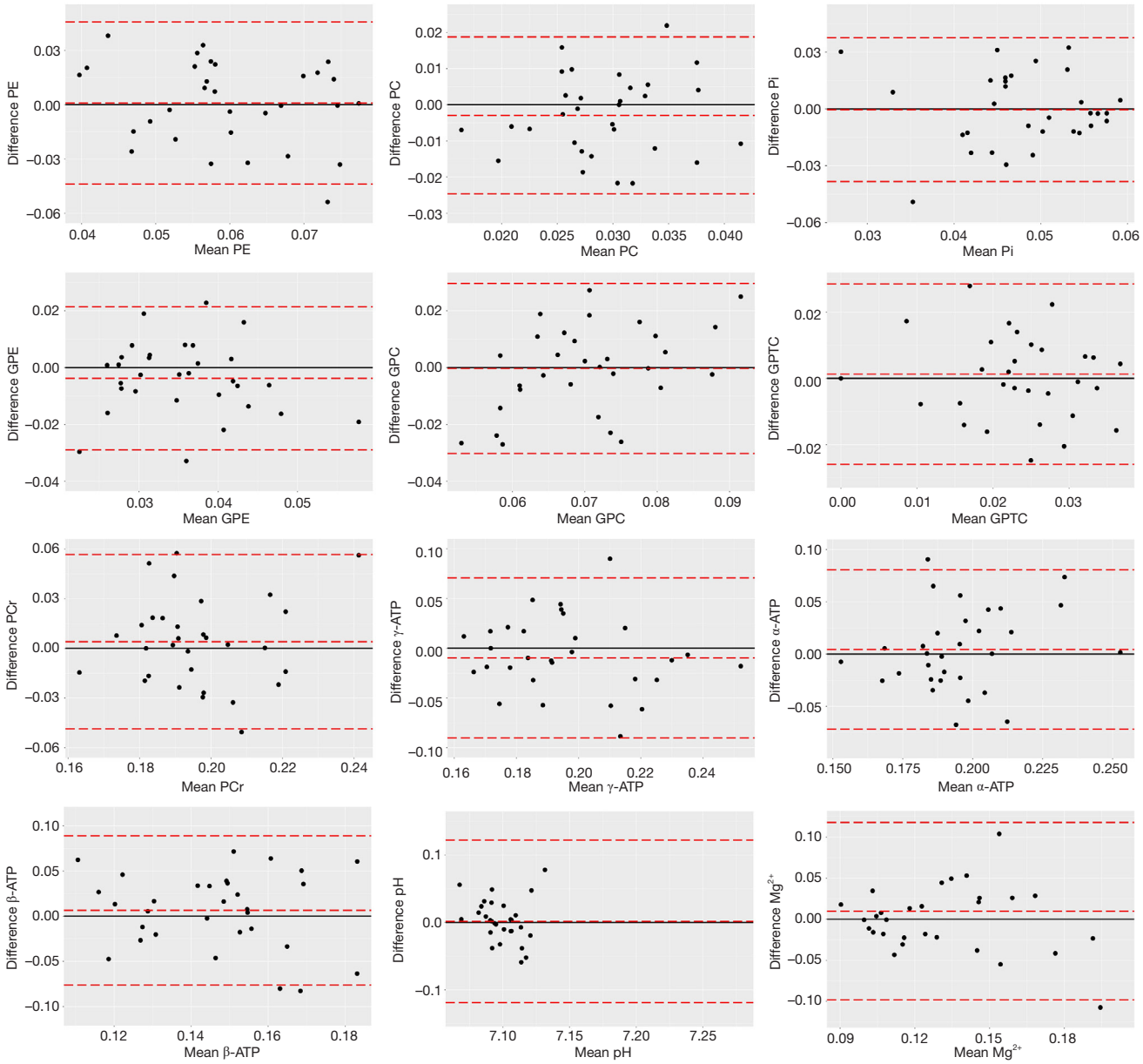

Figure 4 Bland-Altman plots of the two scanned time points of the ^{31}P-MRS metabolites in the thalamus region. All amplitudes were normalized to the total phosphorus signal detected within the respective voxel prior to the statistical analyses. GPE, glycerophosphoethanolamine; GPC, glycerophosphocholine; GPTC, glycerophosphatidylcholine; Mg^{2+}, magnesium ion; MEGA-PRESS, MEscher-GArwood Point RESolved Spectroscopy; PE, phosphoethanolamine; PC, phosphocholine; Pi, inorganic phosphate; PCr, phosphocreatine; γ-, α-, β-ATP, α-, β-, γ-adenosine triphosphate.

Conclusions

This study evaluated the test-retest precision of ^{31}P-MRS and ^{1}H MEGA-PRESS across multiple brain regions using a 3T multi-nuclear MRI system. Intermediate brain regions, such as the temporal lobe and thalamus, showed higher stability than peripheral areas, such as the frontal and occipital lobes. Metabolites such as PCr, ATPs, pH, and Mg^{2+} showed moderate to high stability, rendering them reliable for clinical and research applications. However, PME and PDE metabolites, especially GPTC,

had higher CVs, indicating that their measurements should be interpreted with caution. Glx and GABA+ had better precision than GSH using single-voxel MRS. The findings from this study could enhance the application of ^{31}P-MRS and MEGA-PRESS in neurological research and clinical settings, ensuring precise and reliable brain metabolic evaluations.

Acknowledgments

None.

Footnote

Reporting Checklist: The authors have completed the STARD reporting checklist. Available at https://qims.amegroups.com/article/view/10.21037/qims-24-1853/rc

Funding: This work was supported by the National Key Research and Development Program of China (No. 2022YFC2406903) and the National Natural Science Foundation of China (No. U22A20354).

Conflicts of Interest: All authors have completed the ICMJE uniform disclosure form (available at https://qims.amegroups.com/article/view/10.21037/qims-24-1853/coif). The authors have no conflicts of interest to declare.

Ethical Statement: The authors are accountable for all aspects of the work in ensuring that questions related to the accuracy or integrity of any part of the work are appropriately investigated and resolved. The study was conducted in accordance with the Declaration of Helsinki (as revised in 2013) and approved by the Institutional Review Board of Tongji Hospital of Tongji Medical College of Huazhong University of Science and Technology (No. TJ-IRB20231102). All participants provided written informed consent before the commencement of this study.

References

1. Oz G, Alger JR, Barker PB, Bartha R, Bizzi A, Boesch C, et al. Clinical proton MR spectroscopy in central nervous system disorders. Radiology 2014;270:658-79.
2. Lopez Kolkovsky AL, Carlier PG, Marty B, Meyerspeer M. Interleaved and simultaneous multi-nuclear magnetic resonance in vivo. Review of principles, applications and potential. NMR Biomed 2022;35:e4735.
3. Chance B, Eleff S, Leigh JS Jr. Noninvasive, nondestructive approaches to cell bioenergetics. Proc Natl Acad Sci U S A 1980;77:7430-4.
4. Ackerman JJ, Grove TH, Wong GG, Gadian DG, Radda GK. Mapping of metabolites in whole animals by 31P NMR using surface coils. Nature 1980;283:167-70.
5. Moon RB, Richards JH. Determination of intracellular pH by 31P magnetic resonance. J Biol Chem 1973;248:7276-8.
6. Baeshen A, Wyss PO, Henning A, O'Gorman RL, Piccirelli M, Kollias S, Michels L. Test-Retest Reliability of the Brain Metabolites GABA and Glx With JPRESS, PRESS, and MEGA-PRESS MRS Sequences in vivo at 3T. J Magn Reson Imaging 2020;51:1181-91.
7. Choi IY, Andronesi OC, Barker P, Bogner W, Edden RAE, Kaiser LG, Lee P, Marjańska M, Terpstra M, de Graaf RA. Spectral editing in 1 H magnetic resonance spectroscopy: Experts' consensus recommendations. NMR Biomed 2021;34:e4411.
8. Anton A, Mead RJ, Shaw PJ, Edden RAE, Bigley J, Jenkins TM, Wild JM, Hoggard N, Wilkinson ID. Assessment of the Precision in Measuring Glutathione at 3 T With a MEGA-PRESS Sequence in Primary Motor Cortex and Occipital Cortex. J Magn Reson Imaging 2022;55:435-42.
9. Greenhouse I, Noah S, Maddock RJ, Ivry RB. Individual differences in GABA content are reliable but are not uniform across the human cortex. Neuroimage 2016;139:1-7.
10. Ma RE, Murdoch JB, Bogner W, Andronesi O, Dydak U. Atlas-based GABA mapping with 3D MEGA-MRSI: Cross-correlation to single-voxel MRS. NMR Biomed 2021;34:e4275.
11. Duda JM, Moser AD, Zuo CS, Du F, Chen X, Perlo S, Richards CE, Nascimento N, Ironside M, Crowley DJ, Holsen LM, Misra M, Hudson JI, Goldstein JM, Pizzagalli DA. Repeatability and reliability of GABA measurements with magnetic resonance spectroscopy in healthy young adults. Magn Reson Med 2021;85:2359-69.
12. Hupfeld KE, Zöllner HJ, Hui SCN, Song Y, Murali-

Manohar S, Yedavalli V, Oeltzschner G, Prisciandaro JJ, Edden RAE. Impact of acquisition and modeling parameters on the test-retest reproducibility of edited GABA. NMR Biomed 2024;37:e5076.
13. Song Y, Zöllner HJ, Hui SCN, Hupfeld K, Oeltzschner G, Prisciandaro JJ, Edden R. Importance of Linear Combination Modeling for Quantification of Glutathione and γ-Aminobutyric Acid Levels Using Hadamard-Edited Magnetic Resonance Spectroscopy. Front Psychiatry 2022;13:872403.
14. Matisz CE, Gruber AJ. Neuroinflammatory remodeling of the anterior cingulate cortex as a key driver of mood disorders in gastrointestinal disease and disorders. Neurosci Biobehav Rev 2022;133:104497.
15. Yuan Q, Liang X, Xue C, Qi W, Chen S, Song Y, Wu H, Zhang X, Xiao C, Chen J. Altered anterior cingulate cortex subregional connectivity associated with cognitions for distinguishing the spectrum of pre-clinical Alzheimer's disease. Front Aging Neurosci 2022;14:1035746.
16. Zuo CS, Davis KA, Lukas SE. Lower dACC glutamate in cannabis users during early phase abstinence. Neuropsychopharmacology 2022;47:1969-75.
17. Verveer I, Hill AT, Franken IHA, Yücel M, van Dongen JDM, Segrave R. Modulation of control: Can HD-tDCS targeting the dACC reduce impulsivity? Brain Res 2021;1756:147282.
18. Wijnen JP, Scheenen TW, Klomp DW, Heerschap A. 31P magnetic resonance spectroscopic imaging with polarisation transfer of phosphomono- and diesters at 3 T in the human brain: relation with age and spatial differences. NMR Biomed 2010;23:968-76.
19. Payne T, Burgess T, Bradley S, Roscoe S, Sassani M, Dunning MJ, Hernandez D, Scholz S, McNeill A, Taylor R, Su L, Wilkinson I, Jenkins T, Mortiboys H, Bandmann O. Multimodal assessment of mitochondrial function in Parkinson's disease. Brain 2024;147:267-80.
20. Sassani M, Alix JJ, McDermott CJ, Baster K, Hoggard N, Wild JM, Mortiboys HJ, Shaw PJ, Wilkinson ID, Jenkins TM. Magnetic resonance spectroscopy reveals mitochondrial dysfunction in amyotrophic lateral sclerosis. Brain 2020;143:3603-18.
21. Weber-Fahr W, Englisch S, Esser A, Tunc-Skarka N, Meyer-Lindenberg A, Ende G, Zink M. Altered phospholipid metabolism in schizophrenia: a phosphorus 31 nuclear magnetic resonance spectroscopy study. Psychiatry Res 2013;214:365-73.
22. D'Rozario AL, Bartlett DJ, Wong KKH, Sach T, Yang Q, Grunstein RR, Rae CD. Brain bioenergetics during resting wakefulness are related to neurobehavioral deficits in severe obstructive sleep apnea: a 31P magnetic resonance spectroscopy study. Sleep 2018.
23. Veeraiah P, Jansen JFA. Multinuclear Magnetic Resonance Spectroscopy at Ultra-High-Field: Assessing Human Cerebral Metabolism in Healthy and Diseased States. Metabolites 2023;13:577.
24. Li CW, Negendank WG, Murphy-Boesch J, Padavic-Shaller K, Brown TR. Molar quantitation of hepatic metabolites in vivo in proton-decoupled, nuclear Overhauser effect enhanced 31P NMR spectra localized by three-dimensional chemical shift imaging. NMR Biomed 1996;9:141-55.
25. Lagemaat MW, van de Bank BL, Sati P, Li S, Maas MC, Scheenen TW. Repeatability of (31) P MRSI in the human brain at 7 T with and without the nuclear Overhauser effect. NMR Biomed 2016;29:256-63.
26. Parasoglou P, Osorio RS, Khegai O, Kovbasyuk Z, Miller M, Ho A, Dehkharghani S, Wisniewski T, Convit A, Mosconi L, Brown R. Phosphorus metabolism in the brain of cognitively normal midlife individuals at risk for Alzheimer's disease. Neuroimage Rep 2022;2:100121.
27. Layec G, Bringard A, Le Fur Y, Vilmen C, Micallef JP, Perrey S, Cozzone PJ, Bendahan D. Reproducibility assessment of metabolic variables characterizing muscle energetics in vivo: A 31P-MRS study. Magn Reson Med 2009;62:840-54.
28. Lin A, Andronesi O, Bogner W, Choi IY, Coello E, Cudalbu C, Juchem C, Kemp GJ, Kreis R, Kršňák M, Lee P, Maudsley AA, Meyerspeer M, Mlynarik V, Near J, Öz G, Peek AL, Puts NA, Ratai EM, Tkáč I, Mullins PG; Experts' Working Group on Reporting Standards for MR Spectroscopy. Minimum Reporting Standards for in vivo Magnetic Resonance Spectroscopy (MRSinMRS): Experts' consensus recommendations. NMR Biomed 2021;34:e4484.
29. Edden RA, Puts NA, Harris AD, Barker PB, Evans CJ. Gannet: A batch-processing tool for the quantitative analysis of gamma-aminobutyric acid–edited MR spectroscopy spectra. J Magn Reson Imaging 2014;40:1445-52.
30. Near J, Edden R, Evans CJ, Paquin R, Harris A, Jezzard P. Frequency and phase drift correction of magnetic resonance spectroscopy data by spectral registration in the time domain. Magn Reson Med 2015;73:44-50.
31. Mikkelsen M, Tapper S, Near J, Mostofsky SH, Puts NAJ, Edden RAE. Correcting frequency and phase offsets in MRS data using robust spectral registration. NMR Biomed

2020;33:e4368.
32. Kiebel SJ, Friston KJ. Statistical parametric mapping for event-related potentials (II): a hierarchical temporal model. Neuroimage 2004;22:503-20.
33. Rowland LM, Krause BW, Wijtenburg SA, McMahon RP, Chiappelli J, Nugent KL, Nisonger SJ, Korenic SA, Kochunov P, Hong LE. Medial frontal GABA is lower in older schizophrenia: a MEGA-PRESS with macromolecule suppression study. Mol Psychiatry 2016;21:198-204.
34. Naressi A, Couturier C, Castang I, de Beer R, Graveron-Demilly D. Java-based graphical user interface for MRUI, a software package for quantitation of in vivo/medical magnetic resonance spectroscopy signals. Comput Biol Med 2001;31:269-86.
35. Naressi A, Couturier C, Devos JM, Janssen M, Mangeat C, de Beer R, Graveron-Demilly D. Java-based graphical user interface for the MRUI quantitation package. MAGMA 2001;12:141-52.
36. Rijpma A, van der Graaf M, Meulenbroek O, Olde Rikkert MGM, Heerschap A. Altered brain high-energy phosphate metabolism in mild Alzheimer's disease: A 3-dimensional 31P MR spectroscopic imaging study. Neuroimage Clin 2018;18:254-61.
37. Wilson M, Andronesi O, Barker PB, Bartha R, Bizzi A, Bolan PJ, et al. A Methodological Consensus on Clinical Proton MR Spectroscopy of the Brain: Review and Recommendations. Magn Reson Med 2019;82:527-50.
38. Wijtenburg SA, Near J, Korenic SA, Gaston FE, Chen H, Mikkelsen M, Chen S, Kochunov P, Hong LE, Rowland LM. Comparing the reproducibility of commonly used magnetic resonance spectroscopy techniques to quantify cerebral glutathione. J Magn Reson Imaging 2019;49:176-83.
39. Juchem C, Cudalbu C, de Graaf RA, Gruetter R, Henning A, Hetherington HP, Boer VO. B0 shimming for in vivo magnetic resonance spectroscopy: Experts' consensus recommendations. NMR Biomed 2021;34:e4350.
40. Berrington A, Považan M, Mirfin C, Bawden S, Park YW, Marsh DC, Bowtell R, Gowland PA. Calibration-free regional RF shims for MRS. Magn Reson Med 2021;86:611-24.
41. Hui SCN, Mikkelsen M, Zöllner HJ, Ahluwalia V, Alcauter S, Baltusis L, et al. Frequency drift in MR spectroscopy at 3T. Neuroimage 2021;241:118430.
42. Stein A, Zhu C, Du F, Öngür D. Magnetic Resonance Spectroscopy Studies of Brain Energy Metabolism in Schizophrenia: Progression from Prodrome to Chronic Psychosis. Curr Psychiatry Rep 2023;25:659-69.
43. Shukla D, Mandal PK, Mishra R, Punjabi K, Dwivedi D, Tripathi M, Badhautia V. Hippocampal Glutathione Depletion and pH Increment in Alzheimer's Disease: An in vivo MRS Study. J Alzheimers Dis 2021;84:1139-52.
44. Ren J, Yu F, Greenberg BM. ATP line splitting in association with reduced intracellular magnesium and pH: a brain (31) P MR spectroscopic imaging (MRSI) study of pediatric patients with myelin oligodendrocyte glycoprotein antibody-associated disorders (MOGADs). NMR Biomed 2023;36:e4836.

Cite this article as: Hu S, Yan S, Xie Y, Zhu H, Ding Y, Li Y, Zhang X, Zhu W. Test-retest precision of brain metabolites in healthy participants using ^{31}P-MRS and ^{1}H MEGA-PRESS on a 3T multi-nuclear MRI system. Quant Imaging Med Surg 2025;15(4):2852-2864. doi: 10.21037/qims-24-1853

